Is the transition zone a deep reservoir for fluorine?

Mathilde Roberge, Hélène Bureau, Nathalie Bolfan-Casanova, Daniel J. Frost, Caroline Raepsaet, Suzy Surble, Hicham Khodja, Anne-Line Auzende, Guillaume Fiquet

▶ **To cite this version:**

Mathilde Roberge, Hélène Bureau, Nathalie Bolfan-Casanova, Daniel J. Frost, Caroline Raepsaet, et al.. Is the transition zone a deep reservoir for fluorine?. Earth and Planetary Science Letters, 2015, 429, pp.25-32. 10.1016/j.epsl.2015.07.051 . hal-01191785

HAL Id: hal-01191785

https://hal.sorbonne-universite.fr/hal-01191785v1

Submitted on 2 Sep 2015

HAL is a multi-disciplinary open access archive for the deposit and dissemination of scientific research documents, whether they are published or not. The documents may come from teaching and research institutions in France or abroad, or from public or private research centers.

L'archive ouverte pluridisciplinaire **HAL**, est destinée au dépôt et à la diffusion de documents scientifiques de niveau recherche, publiés ou non, émanant des établissements d'enseignement et de recherche français ou étrangers, des laboratoires publics ou privés.

Is the transition zone a deep reservoir for Fluorine?

Mathilde Roberge[a], Hélène Bureau[a*], Nathalie Bolfan-Casanova[b], Daniel J. Frost[c], Caroline Raepsaet[d], Suzy Surble[d], Hicham Khodja[d], Anne-Line Auzende[a], Guillaume Fiquet[a].

[a] *Institut de Minéralogie, de Physique des Matériaux et de Cosmochimie (IMPMC), Sorbonne Universités – UPMC Univ. Paris 06, CNRS UMR 7590, Muséum National d'Histoire Naturelle, IRD UR 206, 4 place Jussieu, 75252 Paris Cedex 05, France*

[b] *Laboratoire Magmas et Volcans, Université Blaise Pascal, Clermont-Ferrand, France*

[c] *Bayerisches Geoinstitut, Universität Bayreuth, D-95440 Bayreuth, Germany*

[d] *Nanosciences et Innovation pour les Matériaux la Biomédecine et l'Energie / Laboratoire d'Etude des Elements Légers, CEA IRAMIS, CNRS UMR 3299, F-91191 Gif-sur-Yvette, France*

Revised manuscript for

Earth and Planetary Sciences Letters

*Corresponding author.

E-mail address: Helene.bureau@impmc.upmc.fr, Tel. +33 1 44274807

Keywords : fluorine, ringwoodite, wadsleyite, water, solubility, transition zone

Abstract

It is now recognized that the transition zone (TZ) is a significant repository for water. This means that other volatile species may also be stored in this region such as halogen elements. We have measured the solubility of fluorine in wadsleyite (Wd) and ringwoodite (Rw) under hydrous and anhydrous conditions at different pressures and temperatures, relevant for the transition zone. F contents are similar in Wd (665 to 1045 ppm F, up to 956 ppm H_2O) and in Rw (186 to 1235 ppm F, up to 1404 ppm H_2O). This suggests that F may be incorporated in the same manner as water in the major nominally anhydrous minerals of the TZ: ringwoodite and wadsleyite and that the transition zone could be a major reservoir for fluorine. In the framework of the "water filter model" proposed by Bercovici and Karato (2003), the contrast of volatile element contents between a depleted upper mantle and an enriched transition zone could be maintained over geological time scales. Previous estimates of the fluorine content of the Bulk Silicate Earth (BSE), such as 25 ppm by mass, have assumed a homogeneous mantle. Although we do not know whether the TZ is F saturated or not, we used our new experimental data and estimates of the lower mantle F content from ocean island basalts, to estimate a maximum BSE fluorine content of 59 ppm by mass for a hydrous, F-saturated TZ. This upper bound on the range of possible BSE F content emphasizes the challenges when explaining the origin of volatile elements in the Earth from a carbonaceous chondrite late veneer.

1. Introduction

The exceptional finding of a diamond inclusion made of hydrous ringwoodite (Pearson et al., 2014) has definitively proved that the mantle transition zone (410-660 km depth) is a

major deep repository for water. This discovery validates decades of experimental work devoted to the study of the solubility of water in the major nominally anhydrous silicate minerals of the transition zone, wadsleyite and ringwoodite (see the review after Smyth and Jacobsen, 2006). These two phases can host up to 3.3 wt % structural water equivalent (hydroxyl groups), through incorporation processes involving Mg vacancies for ringwoodite (Blanchard et al., 2009) and a combination of Mg and Si vacancies, depending on the water content, for wadsleyite (Blanchard et al., 2013). While the deep water cycle has been extensively studied these last decades, almost nothing is known about the behavior of the most abundant halogen element: fluorine. This element has been intensively studied for igneous processes (see the review after Pyle and Mather, 2009 and references therein), particularly for volcanic degassing (Schilling et al., 1980; Déruelle et al., 1992; Jambon et al., 1995). F affects directly the silicate melt properties such as magma viscosity (Dingwell and Mysen, 1985) or crystallization (Filiberto et al., 2012), and fluorine was for a long time believed to be stored in accessory phases such as phosphates, (apatite) or clinohumite or minor silicate minerals such as amphibole or phlogopite (Smith, 1981). Moreover, fluorine has been shown to be in slight excess in the bulk silicate Earth compared to Carbonaceous Chondrites (McDonough and Sun, 1995). These estimates are based on concentrations measured in natural basalts and peridotites. A direct consequence is that the resulting budget (25 ppm F in the BSE, after McDonough and Sun, 1995) is too high to fulfill a model based on a volatile-rich chondrite origin for the late veneer. Indeed, Marty (2012) has calculated that the contribution of 2% of carbonaceous chondrite material would fulfill the carbon and water abundances of the Earth. This would also fulfill the natural estimated abundances for heavy halogen elements (Cl, Br, I), but the abundance of F requires a much higher contribution of 17%.

For these reasons it seems necessary to determine how F is stored within potential reservoirs of the mantle, and to consider whether the fluorine content in the BSE may have been over or underestimated. Therefore in an attempt to put constrains on the fluorine content in the upper mantle, fluorine concentrations have recently been measured in nominally anhydrous mantle minerals (Beyer et al., 2012; Mosenfelder and Rossman, 2013a, b). These studies have demonstrated that up to 47 ppm of fluorine can be incorporated in natural olivine and pyroxene. By comparison, experimental studies performed to determine fluorine solubility in these major mantle mineral phases yielded maximum contents of fluorine of 4500 ppm to 1900 ppm in olivine (Bromiley and Kohn, 2007; Bernini et al., 2012), 626 ppm in pyroxenes (Dalou et al., 2012), and 1110 ppm in pyrope (Bernini et al., 2012). Like water, that is stored in silicate minerals as hydroxyl species, it has been proposed that the mantle fluorine budget can be entirely accommodated by these mineral phases (Beyer et al., 2012, Crépisson et al., 2014). Based on the observation of clumped fluoride-hydroxyl defects in pure-Mg olivine, the major upper mantle mineral, it is likely that fluorine and water cycles may be strongly coupled through the nominally anhydrous minerals (Crépisson et al., 2014). Like for water, F may be transferred at depth during subduction processes. For example, experimental studies indicate that a dense hydrous magnesium silicate phase - superhydrous phase B - stabilized at subduction zone conditions in the transition zone. This phase might incorporate significant amounts of fluorine and carry it down to the deep mantle (e.g. Hazen et al., 1997). By analogy with water, one may speculate that a significant repository for fluorine may exist in the transition zone (TZ). This is the hypothesis we would like to test in this study.

In this work, we measure the F solubilities in wadsleyite (Wd) and ringwoodite (Rw) to assess the F storage capacity of the TZ. Indeed, it is critical to know to which extent the

potential storage capacity of the transition zone may affect the global F budget and cycle, within a framework whereby F would be continuously brought in the TZ by subduction.

2. Materials and methods

F-bearing olivine, wadsleyite and ringwoodite were synthesized from two different powders: (a) a mixture of MgO, SiO_2, FeO oxides, and (b) a mixture of natural pure San Carlos olivine (Fo_{90}) fine powders mixed with SiO_2. The addition of SiO_2 provides slight excess of silica (Mg/Si atomic ratio =1.76) in order to promote the formation of a silicate melt in equilibrium with the crystals that can incorporate the excess of fluorine and water (Demouchy et al., 2005). F was added as a salt: NaF (up to 5 wt% in the bulk), whereas water was added as brucite in order to get a total amount of 2 wt% H_2O. Mixtures were prepared in order to obtain bulk compositions of about Fo_{90}, corresponding to the pyrolitic composition after Ringwood (1962). Wadsleyite, ringwoodite and olivine were synthesized in a multi-anvil press at pressures between 14 and 22 GPa and in the temperature range 1100°C to 1400°C. Typical run durations were between 30 minutes and 9 hours in either Re, Pt or Au-Pd capsules (Table 1). Experiments were performed at LMV Clermont-Ferrand and BGI Bayreuth following the procedures detailed in (Frost et al., 2001; Demouchy et al., 2005).

Recovered samples were then embedded in crystal bond and mirror polished on one-side. The mineral phases were characterized using Scanning Electron Microscopy (SEM) at IMPMC-UPMC. Mineral identification was realized using Raman spectroscopy. The fine structure of the minerals, imaging, diffraction, and chemical measurements were performed with a JEOL 2100F transmission electron microscope (TEM) with a field emission gun, and

equipped with JEOL EDX detectors at IMPMC (UPMC). The acceleration voltage was at 200 kV and we reached a resolution of 1.8 Å. The samples for TEM were prepared by Focused Ion Beam (FIB) with the dual beam Zeiss Crossbeam Neon 40 ESB at IMPMC (UPMC). The final lamella-thickness obtain is under 100 nm for suitable electron transparency. Major element compositions of the minerals were measured using electron microprobe analyses (EPMA) with an acceleration of 15 kV and 15 µm defocused beam at 10 nA on CAMECA-SX100 at CAMPARIS facility (UPMC, France).

Fluorine and hydrogen contents were measured using ion beam analysis at the nuclear microprobe of the LEEL, CEA, Saclay, France (Khodja et al., 2001). F was measured using Particle Induced Gamma Ray Emission (PIGE) following the procedure described in (Crépisson et al., 2014). Hydrogen was measured using Elastic Recoil Detection Analysis (ERDA) using the procedure described in (Raepsaet et al., 2008; Bureau et al., 2009; Withers et al., 2012).

Before any analysis, the largest crystals were selected with SEM cartographies. PIGE and ERDA measurements have been realized simultaneously with Particle Induced X-Ray Emission (PIXE) and Rutherford Backscattering Spectrometry (RBS) measurements, using a 3x3µm^2 proton beam of 3 MeV for PIGE and a 4x16 µm^2 ^{4}He beam of 3 MeV for ERDA. ERDA analyzes were performed on areas previously analyzed for F.

All measurements were performed by a scanning the beam on large selected areas from 24x50 to 150x100 µm^2. Data acquisitions were performed with a beam current of 500-550 pA, during 1 or 2 hours depending on the concentrations. The combination of RBS and PIXE with ERDA and PIGE was useful to identify the analyzed crystals (Rw, Wd, Ol) and to detect any chemical heterogeneity such as NaF-rich fine intergrowths in the grain boundaries.

Data were first processed using the RISMIN (Daudin et al., 2003) to isolate any chemical heterogeneities and identify the desired crystals, This is possible thanks to the multi-

143 detection system: PIXE, RBS and PIGE allowing the comparison of elemental repartition in
144 the investigated areas, i.e. Na versus F maps, but also Fe and Ca versus F maps, together with
145 SEM pictures of the investigated areas. By comparing the repartitions of these elements we
146 can identify and select (1) Wd, Ol and Rw areas (2) Na not contaminated areas. This is
147 illustrated in the Figure 1 that describes the selection process for sample #3588.

148 After the selection of areas of interest, F and H contents were obtained using
149 SIMNRA software (Mayer, 1997) when PIXE spectra were processed using GUPIXWIN
150 (Campbell et al., 2005) software in order to get concentration with respect to elements of
151 interest such as Fe.

152 PIGE analysis were performed thanks to the quantification of the 197 keV gamma ray
153 emission resulting from $^{19}F(p,p'\gamma)^{19}F$ reaction (Mosbah and Métrich, 1991, Jesus et al., 2000,
154 Habrioux et al., 2012). Na was simultaneously quantified by this method using the 439 keV
155 ray produced by the $^{23}Na(p,p'\gamma)^{23}Na$ reaction. These conditions allow a depth of investigation
156 of about 35 µm for F which is < to the larger size of the investigated crystals except for
157 anhydrous F-bearing minerals. Indeed, when proton beam depth penetration in minerals can
158 effectively reach up to 62 µm owing to the relatively low stopping power of protons, the
159 gamma-ray emission from fluorine is induced only in the beginning of the path, as reaction
160 cross-section falls close to zero for energies under 1.5 MeV as attested by a recent
161 measurement reported in (Jesus et al., 2000).

162 When ERDA is standard less (Raepsaet et al., 2008; Bureau et al., 2009; Withers et al.,
163 2012), the quantification of fluorine requires the use of F-known content samples having a
164 bulk composition similar to the samples (i.e. silicates). Therefore we have used the
165 pantellerite KE12 (4200 ppm F and 5.32 wt% Na, Métrich and Rutherford, 1992) for PIGE
166 calibration. We have preferred this standard instead of a CaF_2 window or a maccusanite glass
167 containing 1.33 wt% F and 3.11wt% Na (Pichavant et al., 1987), because the stopping power

of KE12 is similar to those of our samples. We have used more analysis performed on KE12 and on the Macusanite glass to validate the fluorine quantification. Results obtained for the pantellerite glass KE12 are ranging from 4187 to 4209 ppm F.

3. Results

Samples have been synthesized in multi-anvil press apparatuses from 14 to 22 GPa and from 1100°C to 1400°C (see Materials and methods). This temperature range is relevant for the transition zone and commonly used in experimental studies (e.g. Bolfan-Casanova et al., 2000; Demouchy et al., 2005; Smyth and Jacobsen, 2006). The run durations were ranging from 240 to 420 minutes, except for the references, Wd and Rw free of F and H (20 minutes). No chemical zonation was observed in the investigated crystals and we assume that samples were at chemical equilibrium. Recovered samples contain crystals of Ol, Wd, Rw, depending on the pressure coexisting with clinoenstatite or stishovite, interstitial NaF-rich silicate glass also enriched with respect to H (Table 2). Crystal areas (20 μm^2), are consistently smaller for anhydrous samples, than for hydrous samples, which are typically ~40 μm^2 in average (Fig 2). No particular textural difference or abrupt increase in the amount of quenched melt were observed between hydrous experiments performed at different temperatures.

Transmission Electron Microscopy (TEM) investigation of a thin section containing F-rich Rw (H3588) recovered using focused Ion Beam (FIB) shows that the structure revealed by selected area electron diffraction (SAED) is consistent with a pure single Rw crystal (Fig. 3). This observation also shows that no inclusion of salt or melt is present, and that F and water

191 are incorporated in the crystal lattice. EDX analyses and elemental cartography performed
192 using PIXE (Particle Induced X-Ray Emission) and PIGE (Particle Induced Gamma Ray
193 Emission) do not indicate any chemical heterogeneity in the bulk crystals. Moreover, the Na/F
194 ratios measured by PIGE in Rw and Wd is systematically << 1.21 (NaF ratio), confirming that
195 the detected F is corresponding to a structural concentration and not to the presence of any
196 sub-micron NaF inclusions. Na contents are high, from 713 to 3230, however, such high Na
197 contents have already been reported in wadsleyites (2100-2400 ppm, Gudfinnsson and Wood,
198 1998) synthesized at 1600°C and 14.2 GPa. In these experiments Na_2O was present in the
199 starting materials (a glass) and was not in excess (0.42 wt.% Na_2O).

200 Ol, Wd and Rw compositions range from Fo_{88} to Fo_{97} (with Fo defined as
201 100*(Mg/(Mg+Fe)), while F contents, determined by PIGE, range from 323 to 410 ppm F for
202 Ol, from 665 to 1045 ppm F for Wd and from 186 to 1235 ppm F for Rw (Table 1). The
203 detection limit for F ranges from 37 to 123 ppm F for any investigated phase. The highest F
204 contents are found in anhydrous Wd and Rw (Table 1). With the exception of run H3695, Wd
205 and Rw F contents are higher than those of Ol (Table 1). Water contents measured by using
206 Elastic Recoil Detection Analysis (ERDA), amount 428 H_2O for Ol, whereas 864 to 956 ppm
207 H_2O are detected in Wd and 854 to 1404 ppm H_2O are measured for Rw (Table 1).

208 When comparing different temperatures of synthesis, a slight decrease of F content is
209 observed with increasing temperature in hydrous Rw. We do not have enough results to
210 determine if a temperature effect would affect the F content of both Rw and Wd, similarly to
211 what as it has been shown for water contents in Wd by Demouchy and co-workers (2005, see
212 Fig 4). Figure 5 shows that the highest F contents are associated with quasi-anhydrous
213 minerals when fluorine is examined as a function of H_2O.

214

215 **4. Discussion**

4.1 Water and Fluorine in Ringwoodite and Wadseyite

For volatile elements, solubility measurements, i.e. determination of the maximum content of the element in a matrix (silicates minerals, melts), have been used for decades to understand deep processes such as magma degassing, partial melting and physical properties or to assess to mantle storage. Thus determining the upper limits of volatile contents is key to making progress in the understanding of volatile element cycling into the Earth.

We show an H_2O solubility contrast for Ol (up to 428 ppm) compared with Wd and Rw (from 854 to 1404 ppm) with more water dissolved in the two high-pressure phases. This is in agreement with previous studies (e.g. Bolfan-Casanova et al., 2000; Ohtani et al., 2001; Demouchy et al., 2005;) but the amount of water measured in Wd and Rw from this study is one order of magnitude lower than previously reported solubilities for these phases (up to 3 wt.% e.g. Smyth and Jacobsen, 2006). Such a significant reduction of OH incorporation is likely attributed to the presence of NaF salt which will reduce the H_2O activity in the melt in equilibrium with the mineral phases. Previous studies have observed a significant decrease of OH incorporation in enstatite (2.5 GPa and 1150-1400°C), linked to the increase of NaCl or KCl content in starting materials (Stalder et al., 2008). An additional possibility might be a competition process between OH and F for incorporation in the mineral lattices of Wd and Rw. Indeed, a recent study combining infrared characterization of experimentally F- and OH-enriched olivines and first-principle calculations, Crépisson and co-workers (2014) have demonstrated a close association of fluoride, hydroxyl groups and Si vacancies. They found evidence for the presence of clumped fluoride-hydroxyl defects in the forsterite structure. Whereas in NaF-free systems the proposed H_2O incorporation mechanism mostly involves Mg vacancies in forsterite (*e.g* Balan et al., 2011) and in ringwoodite (Blanchard et al., 2009). Blanchard et al. (2013) have also provided evidence for the association of hydroxyl groups with Si vacancies in H_2O-rich wadsleyites. Assuming that F and OH share the same vacancies

241 in Wd and Rw, and considering the slight F content decrease associated with increasing SiO_2
242 contents (Fig 6), we propose that F may at least partially be associated with Si vacancies. This
243 suggests that H_2O and F cycles are linked in the upper mantle and TZ, through Ol, Wd and
244 Rw.

245 F solubilities measured in Rw (186-1235 ppm) and in Wd (665-1045 ppm) are similar
246 for both phases and higher than any F concentrations measured in natural NAMs of the upper
247 mantle. A comparison with previous experimental studies is moreover difficult because
248 experimental conditions are not consistent between studies (pressures, bulk compositions,
249 starting materials). Very high F contents experimentally obtained in olivines (e.g. in the 2-4
250 GPa pressure range: 1715 ppm F, Crépisson et al., 2014), would suggest a possible pressure
251 effect on F solubility.

252

253 *4.2 Fluorine in the transition zone*

254 From the lithophile behavior of F (McDonough and Sun, 1995) and based on previous
255 studies (Beyer et al., 2012), it has been proposed that nominally anhydrous silicate phases
256 (such as olivine and pyroxene Px) might accommodate the bulk F content of the whole upper
257 mantle in regards to their high modal proportion in the mantle. However, the F contents
258 measured in upper mantle natural Ol and Px are < 100 ppm (Hervig and Bell, 2005; Beyer et
259 al., 2012; Mosenfelder and Rossman 2013a, b). Here we show that Wd and Rw are potentially
260 important F-bearing minerals, and that the TZ is a good candidate for its storage for two
261 reasons: (1) fluorine may have been trapped very early in the TZ when the mantle was
262 crystallizing from the magma ocean; (2) fluorine may be regularly supplied to the TZ through
263 subduction. Indeed, a regular water supply is expected from the slabs. F is lithophile
264 compared to Cl, Br and I, which are hydrophilic (e.g. Bureau et al., 2000; 2010), therefore

265 when most of the heavy halogen elements and a significant part of water are likely
266 devolatilized from the slab during dehydration processes, most of the F may remain in the
267 slabs en route to the TZ. Subduction would thus drive an annual global flux of 8.7×10^{14} g
268 H_2O (Peacock, 1990) and of 9.9-10x10^{12} g F to the Earth's interior (John et al., 2011). Large
269 amounts of F and water are expected to be recycled back to the mantle (95% F and 87% water
270 respectively, Peacock, 1990; John et al., 2011). Hydrous phases may transport F efficiently to
271 the TZ (e.g. Hazen et al., 1997). Once the subducted slab reaches the TZ, the storage of F and
272 water would be enhanced by the tendency of many slabs to deflect horizontally, and to remain
273 permanently or temporarily at the 660-km discontinuity (e.g. Fukao et al., 2001).

274 It has been proposed that a neutral buoyant hydrous melt phase on the top of the TZ (410
275 km depth) could control the distribution of incompatible elements within the upper mantle,
276 acting as a chemical filter, the so-called "water-filter" model (Bercovici and Karato, 2003). In
277 this model a high water content within the range 0.2 – 2 wt.% is assumed in the TZ, which is
278 consistent with the 1 wt. % of water measured in a natural diamond inclusion of ringwoodite
279 (Pearson et al., 2014). The water dissolved in the mantle would create a thin layer of melt at
280 410 km depth, corresponding to the transformation of Wd into Ol and a hydrous melt (Fig 7).
281 This dehydration melting would create a 10 km thick layer of molten silicate just above the
282 410-km discontinuity that would retain most of the water together with incompatible
283 elements. Since the melt is denser than the TZ minerals at these pressures it would remain
284 stable. In this view of the mantle, the layer of melt would act as a filter by removing elements
285 rising from the deep mantle and keeping the upper mantle chemically depleted and anhydrous
286 (Bercovici and Karato, 2003). Following this model, the TZ is enriched in water and fluorine
287 even when the upper mantle is depleted.

288

289 *4.3 The Fluorine budget in the Bulk Silicate Earth*

290

291 Our new experimental data allow us to estimate an upper bound for the BSE content of
292 F assuming that the TZ is hydrous and saturated in F. We have calculated a maximum value
293 for the BSE content of F assuming that the TZ is hydrous and saturated in F. We have used
294 the F content of 16 ppm for the lower mantle, determined by (Beyer et al., 2012) from the
295 concentrations of F measured in melt inclusions trapped in olivines from OIB products, when
296 the degree of melting is of 2%. The crust is believed to contain 553 ppm F (Rudnick and Gao,
297 2003), the depleted mantle (TZ excluded) is expected to host 12 ppm F (Beyer et al.,
298 2012). This F content, inferred from its concentration in Ol and orthopyroxene in spinel
299 lherzolites, is in good agreement with the F concentration proposed for the depleted MORB
300 mantle (11 ppm F, Salters and Stracke, 2004). The calculated primitive OIB source is
301 supposed to contain 16 ppm F (17 ppm including a contamination by 3% of recycled crust)
302 based on the measurement of natural OIB volcanic samples (Beyer et al., 2012). In addition,
303 OIBs are assumed to be not affected in their ascent through the TZ (Bercovici and Karato,
304 2003). In order to calculate the maximum amount of F in the TZ, we have used an average
305 pyrolite mineral assemblage model, together with the F contents obtained in our experiments
306 for Wd and Rw of mantle composition (Mg# 0.90, Table 1). We assume a high F content for
307 Rw and Wd as a first approximation for the upper limit of the F BSE content. This is based on
308 the recent discovery of high water content (1.5 wt.%) in a ringwoodite trapped in a natural
309 diamond (Pearson et al., 2014) and makes the assumption that the OH and F cycles are linked
310 in silicate minerals. This assumption needs to be verified by further studies, such as
311 partitioning measurements, and the maximum F content in the TZ may be reconsidered later.
312 We have also assumed that F contents in clinopyroxene, garnet and Ca-perovskite are not
313 significant.

We obtain a value of 23.8×10^{22} g F for the BSE corresponding to 59 ppm F (Fig 7). This high limit value is twice higher than the previous calculation of 25 ppm F after McDonough and Sun (1995), calculated from the Fluorine contents of MORBs and based on a homogeneous mantle. If the BSE contained this higher (59 ppm) amount of Fluorine, this would mean that about 70% of Earth's total fluorine budget would be currently stored in the transition zone. Assuming the present-day flux for F recycling into the mantle (John et al., 2011, fig. 7), more than 16 billion years would be necessary to fill the transition zone by subduction recycling if the TZ if it contained the maximum value of 16.8×10^{22} g of F. As discussed above, the fluorine content of the bulk silicate Earth is probably in the range 25 to 59 ppm and most of the mantle's fluorine is probably stored in the transition zone. If all these assumptions are correct, it would mean that, F was stored in the TZ during the crystallization of the magma ocean during the Earth's differentiation in the Hadean. This is possible if we assume that the “water-filter” model (Bercovici and Karato, 2003) is an efficient process for F retention in the mantle and consequently a key control on the abundance of F in the Earth’s crust.

The Earth is the result of possibly complex accretion and differentiation processes. The primordial building material for the Earth is still the matter of strong debates (e.g. Marty, 2012; Javoy, 1995; Albarède, 2009) especially with respect to volatile elements. Considering the BSE contents in volatile elements after (McDonough and Sun, 1995) and comparing them with the abundances of the carbonaceous chondrites (CC: the most primitive materials), it has been shown that fluorine is slightly enriched compared to heavy halogen elements (Cl, Br, I) and noble gases. Indeed, if hydrogen, carbon and heavy halogen contents would be obtained after the addition of 2 % of a CC late veneer, it would be necessary to add 17% mass of a carbonaceous chondrite to reach the observed BSE fluorine amount (Marty, 2012). This would been even worse if the BSE would content more than 25 ppm. This also emphasizes

339 the fact that the origin of F in the Earth is difficult to explain with the simple accretion of CI
340 chondrites during the differentiation stage.

341

342 Our measurements show that a significant amount of fluorine could be stored in the
343 transition zone, and we suggest that the global F budget of the Earth may have been
344 underestimated. More experimental data are necessary to constrain the fluorine cycle and
345 storage in the Earth.

346 **5. Conclusion**

347

348 We have shown that the fluorine solubility in Wd and Rw is high at water contents,
349 pressures and temperatures relevant to the TZ. Therefore, we suggest that F may be
350 significantly stored together with water in the TZ. The association of F and H_2O shows that
351 their two geochemical cycles are associated at least through their incorporation in nominally
352 anhydrous minerals. Assuming that 95% of the subducted F is recycled back to the mantle, a
353 significant amount of F would reach the TZ where the slab is believed to be stagnant. In this
354 way the TZ would be continuously supplied in F and water by subduction processes. In the
355 frame of the "water-filter model" at the top of the TZ, both F and water contents may be
356 chemically zoned in the mantle at a steady state. The global content of F in the bulk silicate
357 Earth is probably underestimated. Assuming a hydrous, F-saturated TZ, we calculate an upper
358 limit for the BSE F content of 59 ppm wt., higher than the previous estimate of 25 ppm by
359 mass assuming a homogeneous mantle (McDonough and Sun, 1995). It is not know whether
360 the TZ is F-saturated but given this uncertainty we propose that BSE fluorine content is better
361 quoted as being in the range between 25 and 59 ppm by mass. If a significant amount of F is
362 stored in the TZ, it puts constrains on the models proposed to explain the origin of volatile

elements in the Earth. We also suggest that the actual BSE content estimated for the heavy halogen elements chlorine, bromine and iodine may need to be revised, because these elements would also likely been stored in the mineral assemblage of the TZ, but their real contents in deep minerals remain unknown. A real progress in the understanding of the origin of volatile elements requires the determination of precise budgets for these elements in the whole Earth.

Acknowledgments

The authors thank the staff from the nuclear microprobe LEEL CEA Saclay and the staff from BGI Bayreuth for their constant support during the course of this research. Special thanks to H. Schulze for the careful sample preparation. We warmly thank I. Estève for her assistance during SEM analysis and for FIB section preparation. We are grateful to J.C. Boulliard who provided samples from the mineralogical collection of UPMC, and to O. Beyssac for access to the Raman spectrometer. We thank D. Pinti for a constructive examination of the early manuscript. The manuscript has been greatly improved thanks to the constructive reviews and comments from the Editor T. Mather and two anonymous reviewers. The FIB and SEM facility of IMPMC which is supported by Région Ile de France Grant SESAME 2006 NOI-07-593/R, INSU-CNRS, INP-CNRS, UPMC, and by the French National Research Agency (ANR) Grant ANR-07-BLAN-0124-01. We thank the LEEL staff who helped us during PIGE and ERDA sessions. The present study was supported by Campus France through the PROCOPE Project 26673WC (H. Bureau) and the DFG grant 54366326 (D.J. Frost).

References

Albarède F., 2009. Volatile accretion history of the terrestrial planets and dynamic implications, Nature, 461, 7268, 1227-1233.

Balan E., Ingrin J., Delattre S., Kovács I., Blanchard M., 2011. Theoretical infrared spectrum of OH-defects in forsterite, Eur. J. Mineral., 23, 285-292.

Bercovici D., Karato S., 2003. Whole-mantle convection and the transition-zone water filter, Nature, 425, 39‑44.

Bernini D., Wiedenbeck M., Dolejš D., and Keppler H., 2012. Partitioning of halogens between mantle minerals and aqueous fluids: implications for the fluid flow regime in subduction zones, Contrib. Mineral. Petrol., 165, 117-128.

Beyer C., Klemme S., Wiedenbeck M., Stracke A., Vollmer C., 2012. Fluorine in nominally fluorine-free mantle minerals: Experimental partitioning of F between olivine, orthopyroxene and silicate melts with implications for magmatic processes, Earth Planet. Sci. Lett., 337-338, 1-9.

Blanchard M., Balan E., Wright K., 2009. Incorporation of water in iron-free ringwoodite: A first-principles study, Am. Mineral., 94, 83-89.

Blanchard M., Roberge M., Balan E., Fiquet G., Bureau H., 2013. Infrared signatures of OH-defects in wadsleyite: A first-principles study, Am. Mineral., 98, 2132-2143.

Bolfan-Casanova N., Keppler H., Rubie D. C., 2000. Water partitioning between nominally anhydrous minerals in the MgO–SiO_2–H2O system up to 24 GPa: implications for the distribution of water in the Earth's mantle, Earth Planet. Sci. Lett., 182, 209-221.

412 Bromiley D.W., Kohn S.C., 2007. Comparisons between fluoride and hydroxide
413 incorporation in nominally anhydrous and fluorine-free mantle minerals. Geochim.
414 Cosmochim. Acta, 71 Sup. A124.
415 Bureau H., Keppler H., Métrich N., 2000. Volcanic degassing of bromine and iodine:
416 experimental fluid/melt partitioning data and applications to stratospheric chemistry,
417 Earth Planet. Sci. Lett., 183, 51-60.
418 Bureau H., Foy E., Raepsaet C., Somogyi A., Munsch P., Simon G., Kubsky S., 2010.
419 Bromine cycle in subduction zones through in situ Br monitoring in diamond anvil cells,
420 Geochim. Cosmochim. Acta, 74, 3839-3850.
421 Bureau H., Raepsaet C., Khodja H., Carraro A., Aubaud C., 2009. Determination of hydrogen
422 content in geological samples using elastic recoil detection analysis (ERDA), Geochim.
423 Cosmochim. Acta, 73, 3311-3322.
424 Campbell J.L., Maxwell J.A., Teesdale W.J., 2005. The guelph-pixe software package-II.
425 Nucl. Instrum. Methods B, 95, 407-421.
426 Crépisson C., Blanchard M., Bureau H., Sanloup C., Withers A. C., Khodja H., Surblé S.,
427 Raepsaet C., Béneut K., Leroy C., Giura P., Balan E., 2014. Clumped fluoride-hydroxyl
428 defects in forsterite: Implications for the upper-mantle, Earth Planet. Sci. Lett., 390, 287-
429 295.
430 Dalou C., Koga K. T., Shimizu N., Boulon J., Devidal J.-L., 2012. Experimental
431 determination of F and Cl partitioning between lherzolite and basaltic melt, Contrib.
432 Mineral. Petrol., 163, 591-609.
433 Daudin L., Khodja H., Gallien J.-P., 2003. Development of “position–charge–time” tagged
434 spectrometry for ion beam microanalysis. Nucl. Instrum. Methods Phys. Res. B, 210,
435 153–158.

436 Demouchy S., Deloule E., Frost D. J., Keppler H., 2005. Pressure and temperature-
437 dependence of water solubility in Fe-free wadsleyite, Am. Mineral., 90, 1084-1091.
438 Déruelle B., Dreibus G., Jambon A., 1992. Iodine abundances in oceanic basalts: implications
439 for Earth dynamics, Earth Planet. Sci. Lett., 108, 217-227.
440 Dingwell D. B. and Mysen B. O., 1985. Effects of water and fluorine on the viscosity of albite
441 melt at high pressure: a preliminary investigation, Earth Planet. Sci. Lett., 74, 266-274.
442 Filiberto J., Wood J., Dasgupta R., Shimizu N., Le L., Treiman A. H., 2012. Effect of fluorine
443 on near-liquidus phase equilibria of a Fe–Mg rich basalt, Chem. Geol., 312-313, 118-
444 126.
445 Frost D. J., Langenhorst F., van Aken P. A., 2001. Fe–Mg partitioning between ringwoodite
446 and magnesiowüstite and the effect of pressure, temperature and oxygen fugacity, Phys.
447 Chem. Miner., 28, 455-470.
448 Fukao Y., Widiyantoro S., Obayashi M., 2001. Stagnant slabs in the upper and lower mantle
449 transition region, Rev. Geophys., 39, 291–323.
450 Habrioux A., Surble S., Berger P., Khodja H., D'Affroux A., Mailley S., Gutel T., Patoux S.
451 2012. Nuclear microanalysis of lithium dispersion in $LiFePO_4$ based cathode materials
452 for Li-ion batteries. Nucl. Instrum. Methods Phys. Res. B, 290, 13–18.
453 Hazen R. M., Yang H., Prewitt C. T., Gasparik T., 1997. Crystal chemistry of superfluorous
454 phase B ($Mg_{10}Si_3O_{14}F_4$); implications for the role of fluorine in the mantle, Am.
455 Mineral., 82, 647-650.
456 Hervig R.L., Bell D.R. 2005. Fluorine and hydrogen in mantle megacrysts. AGU, Fall
457 Meeting 2005, abstract #V41A-1426.
458 Gudfinnsson G.H., Wood B.J., 1998. The effect of trace elements on the olivine-wadsleyite
459 transformation, Am. Mineral., 83, 1037-1044.

460 Jambon A., Déruelle B., Dreibus G., Pineau F., 1995. Chlorine and bromine abundance in
461 MORB: the contrasting behaviour of the Mid-Atlantic Ridge and East Pacific Rise and
462 implications for chlorine geodynamic cycle, Chem. Geol., 126, 101-117.
463 Javoy M., 1995. The integral enstatite chondrite model of the Earth, Geophys. Res. Lett., 22,
464 2219–2222.
465 Jesus A.P., Braizinha B., Ribeiro J.P., 2000. Excitation function and cross-sections of the
466 reaction $^{19}F(p,p'\gamma)^{19}F$. Nucl. Instrum. Methods Phys. Res. B, 161-163, 186-190.
467 John T., Scambelluri M., Frische M., Barnes J. D., Bach W., 2011. Dehydration of subducting
468 serpentinite: Implications for halogen mobility in subduction zones and the deep halogen
469 cycle, Earth Planet. Sci. Lett., 308, 65-76,
470 Khodja H., Berthoumieux E., Daudin L., Gallien J.-P., 2001. The Pierre Süe Laboratory
471 nuclear microprobe as a multi-disciplinary analysis tool, Nucl. Instrum. Methods Phys.
472 Res. B , 181, 83-86.
473 Marty B., 2012. The origins and concentrations of water, carbon, nitrogen and noble gases on
474 Earth, Earth Planet. Sci. Lett., 313-314, 56-66.
475 Mayer, M., 1997. SIMNRA User's Guide. Report IPP 9/113, Max-Planck-Institut für
476 Plasmaphysik, Garching, Germany.
477 McDonough W. F., Sun S., 1995. The composition of the Earth, Chem. Geol., 120, 223-253.
478 Métrich N., Rutherford M. 1992. Experimental-Study of Chlorine Behavior in Hydrous Silicic
479 Melts. Geochim. Cosmochim. Acta 56, 607–616.
480 Mosbah M, Métrich N., 1991. PIGME fluorine determination using a nuclear microprobe with
481 application to glass inclusions. Nucl. Instrum. Methods Phys. Res. B, 58, 227-231.
482 Mosenfelder J. L., Rossman G. R., 2013a. Analysis of hydrogen and fluorine in pyroxenes: I.
483 Orthopyroxene, Am. Mineral., 98, 1026-1041.

Mosenfelder J. L., Rossman G. R., 2013b. Analysis of hydrogen and fluorine in pyroxenes: II. Clinopyroxene , Am. Mineral., 98, 1042-1054.

Ohtani E., Toma M., Litasov K., Kubo T., Suzuki A., 2000. Stability of dense hydrous magnesium silicate phases and water storage capacity in the transition zone and lower mantle, Phys. Earth Planet. Inter., 124, 105-117.

Peacock S. A., 1990. Fluid Processes in Subduction Zones, Science, 248, 329-337.

Pearson D. G., Brenker F. E., F. Nestola, McNeill J., Nasdala L., Hutchison M. T., Matveev S., Mather K., Silversmit G., Schmitz S., Vekemans B., Vincze L., 2014. Hydrous mantle transition zone indicated by ringwoodite included within diamond, Nature, 507, 221-224.

Pichavant M., Valencia-Herrera J., Boulmier S., Briqueu L., 1987. The Macusani glasses S.E. Peru : evidence of chemical fractionation in peraluminous magmas, in “Magmatic processes : physico-chemical principles. Geochem. Soc. 1, 359–373.

Pyle D. M. and Mather T. A., 2009. Halogens in igneous processes and their fluxes to the atmosphere and oceans from volcanic activity: A review, Chem. Geol., 263, 110-121.

Raepsaet C., Bureau H., Khodja H., Aubaud C., Carraro A. , 2008. Micro-ERDA developments in order to improve the water content determination in hydrous and nominally anhydrous mantle phases. Nucl. Instrum. Methods Phys. Res. B, 266, 1333–1337.

Ringwood A. E., A model for the upper mantle, J. Geophys. Res., 67, 857-867.

Rudnick R. L., Gao S., 2003. Composition of the Continental Crust, in Treatise on Geochemistry, Elsevier, 1-64.

Salters V. J. M., Stracke A., 2004. Composition of the depleted mantle, Geochem. Geophys. Geosystems, 5.

508 Schilling J.-G., Bergeron M. B., Evans R., Smith J. V., 1980. Halogens in the Mantle Beneath
509 the North Atlantic, Philos. Trans. R. Soc. London 297, 147-178.
510 Smith J. V., 1981. Halogen and phosphorus storage in the Earth, Nature, 289, 762-765.
511 Smyth J.R, Jacobsen S.D., 2006.Nominally anhydrous Minerals and Earth's deep Water
512 Cycle, in Earth's Deep Water Cycle, Ed. S. D. Jacobsen and S. Van der Lee Eds. AGU
513 Monography, 1-11.
514 Stalder R., Kronz A., Simon K., 2008. Hydrogen incorporation in enstatite in the system
515 $MgO–SiO_2–H_2O–NaCl$, Contrib. Mineral. Petrol., 156, 653-659.
516 Straub, S.M., and Layne, G.D. 2003. The systematics of chlorine, fluorine, and water in Izu
517 arc front volcanic rocks: Implications for volatile recycling in subduction zones. Geochim.
518 Cosmochim. Acta 67, 4179–4203.
519 Withers A. C., Bureau H., Raepsaet C., Hirschmann M. M., 2012. Calibration of infrared
520 spectroscopy by elastic recoil detection analysis of H in synthetic olivine, Chem. Geol.,
521 334, 92-98.

522 **Figure captions**

523

524 **Fig.1:** Sample #3588 of ringwoodite: SEM picture, PIGE spectrum showing the F peak
525 located at 197 keV. Larger grain sizes are of about 80 µm. 100*100 μm^2 maps of element
526 repartition in the selected area of interest, corresponding to one large crystal of ringwoodite:
527 Fe from PIXE, Na and F from PIGE, Mg from RBS. Hot spots in the maps are corresponding
528 to interstitial NaF-bearing silicate glasses.

529 **Fig. 2:** SEM pictures of hydrous and anhydrous ringwoodites showing the difference in
530 crystal sizes: about 10 µm for anhydrous Rw and about 40 µm for hydrous Rw. Anhydrous F
531 Rw, sample H3567 ; B Hydrous F Rw, sample H3696

532

533 **Fig. 3:**

534 A) SEM image of ringwoodite sample H3588. The thick grey line shows the position where a
535 FIB section has been dig.
536 B) Bright field image and the corresponding diffraction pattern C) of the Rw crystal
537 investigated. No evidence of nano-inclusion is observed.

538

539 **Fig. 4:**

540 F content in ppm wt. plotted versus temperature. A slight decrease of F content is observed
541 with the temperature increase for Rw whereas it seems to have no effect on the F content of
542 Wd.
543 Circles: Ol, squares: Wd, triangles : Rw. Black symbols are for anhydrous samples, open
544 symbols are for hydrous samples.

Fig. 5:

F ppm wt. plotted versus water ppm wt. contents. The highest F contents are associated with quasi anhydrous minerals, but a slight increase of fluorine content is associated to an increase of water in Rw. Symbols as in Figure 3.

Fig. 6:

F ppm wt. plotted versus SiO_2 wt. % contents. The highest F contents are associated with the lowest SiO_2 concentrations in ringwoodites possibly in wadsleyites. Assuming a similar incorporation processes for F in close association with OH in Wd and Rw, than in Ol, one may suggest an incorporation in Si vacancies. Symbols as in Figure 3.

Fig 7:

Schematic section of the interior of the Earth showing F storage and fluxes. Yellow arrows show F and H fluxes: estimated fluxes of HF released to the atmosphere (Pyle et Mather, 2009) and subducted F (John et al., 2011) and H (Straub and Layne, 2003) fluxes. Distribution of F in the mantle is from this study. In this model the TZ is enriched both in F and H. T This region of the mantle may control the distribution of these two volatile elements via the "water filter" model (Bercovici and Karato, 2003).

Fig 1

SEM picture of sample #3588

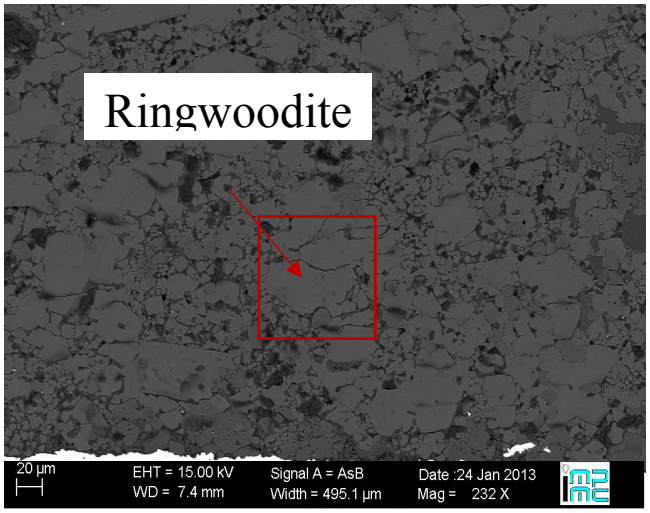

PIGE

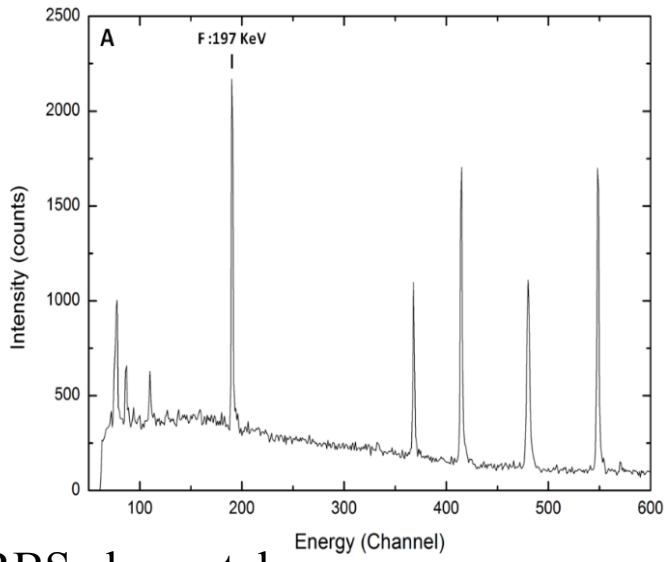

PIXE, PIGE and RBS elemental

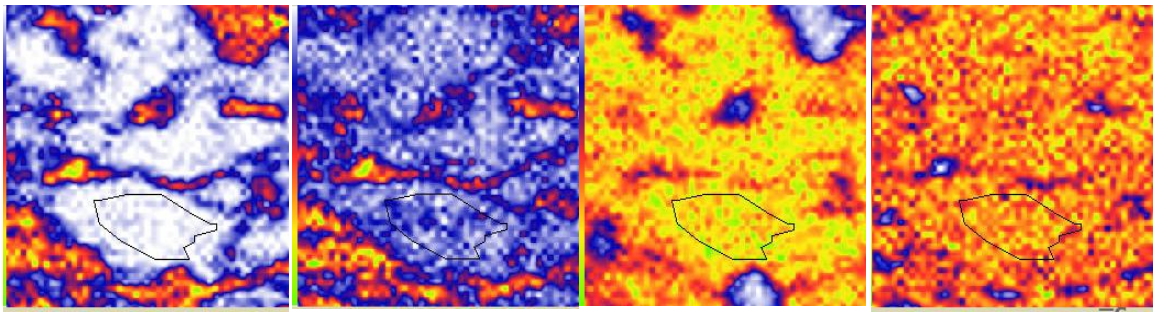

Na F Fe Mg

Fig 2

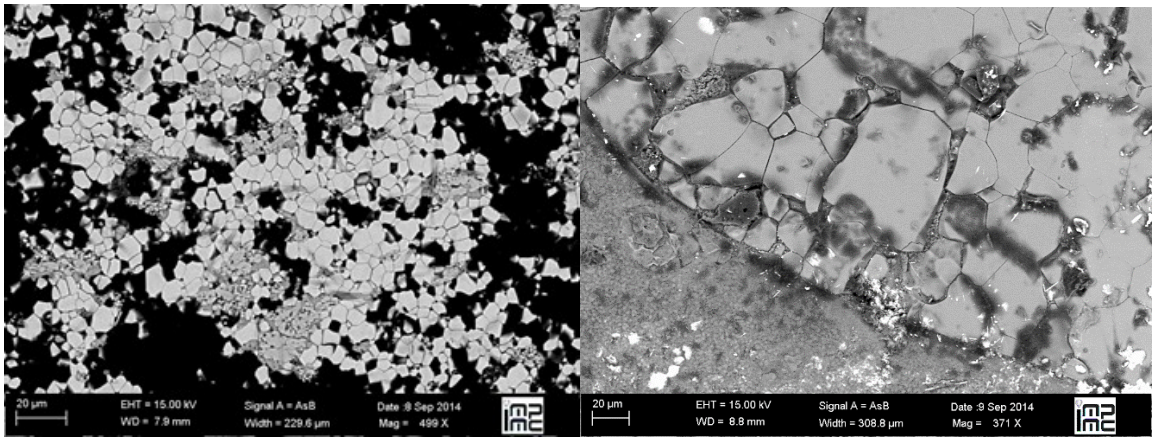
20 µm
EHT = 15.00 kV
WD = 7.9 mm
Signal A = AsB
Width = 229.6 µm
Date :8 Sep 2014
Mag = 499 X
20 µm
EHT = 15.00 kV
WD = 8.8 mm
Signal A = AsB
Width = 308.8 µm
Date :9 Sep 2014
Mag = 371 X

Fig 3

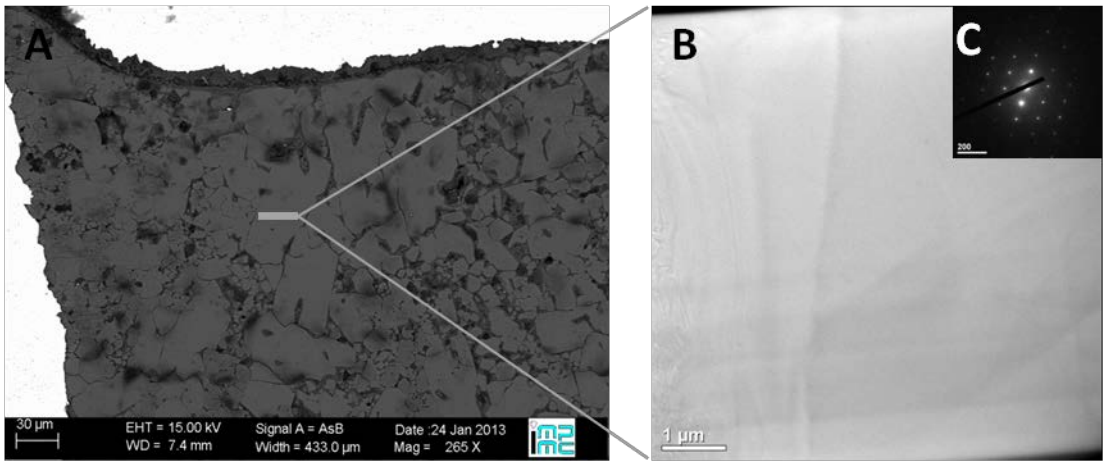
A
30 µm
EHT = 15.00 kV
WD = 7.4 mm
Signal A = AsB
Width = 433.0 µm
Date :24 Jan 2013
Mag = 265 X
B
1 µm
C
200

Fig 4

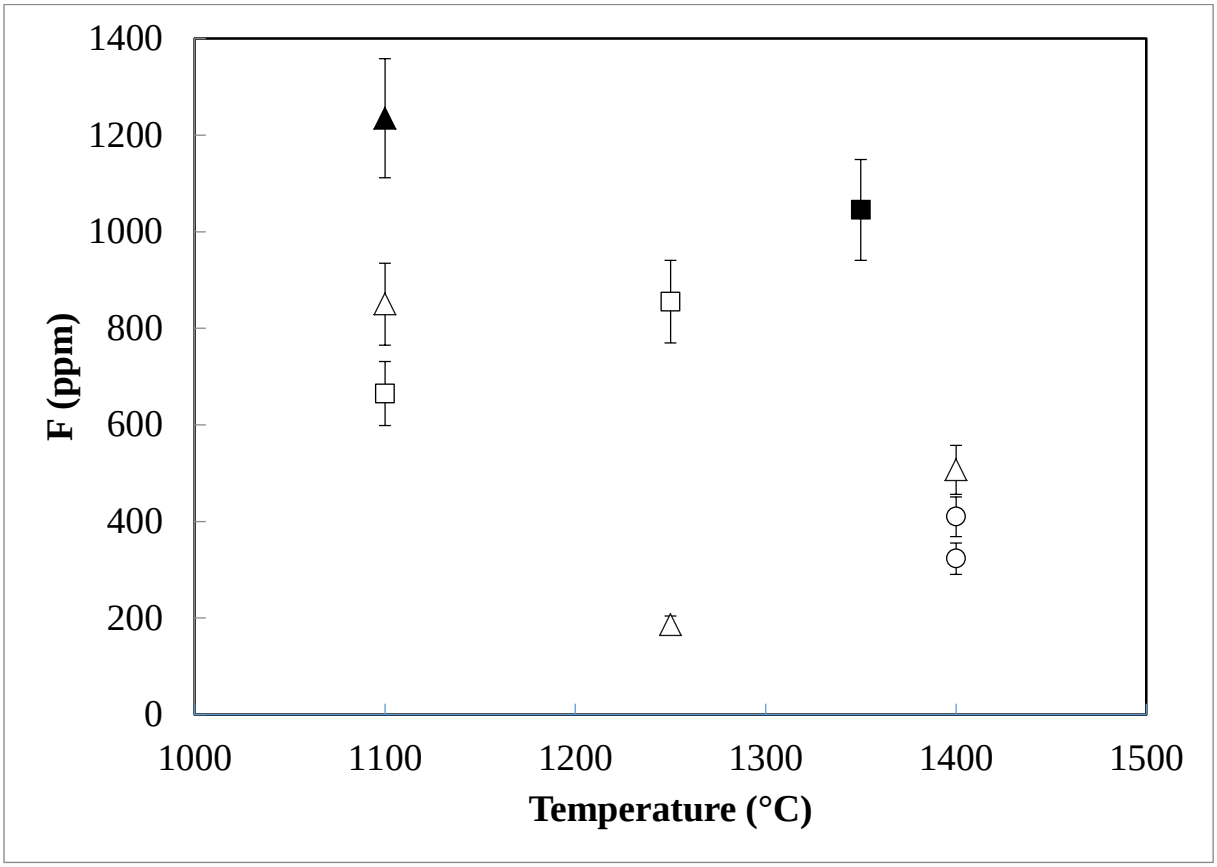
1400
1200
1000
800
600
400
200
0
F (ppm)
1000
1100
1200
1300
1400
1500
Temperature (°C)

Fig 5

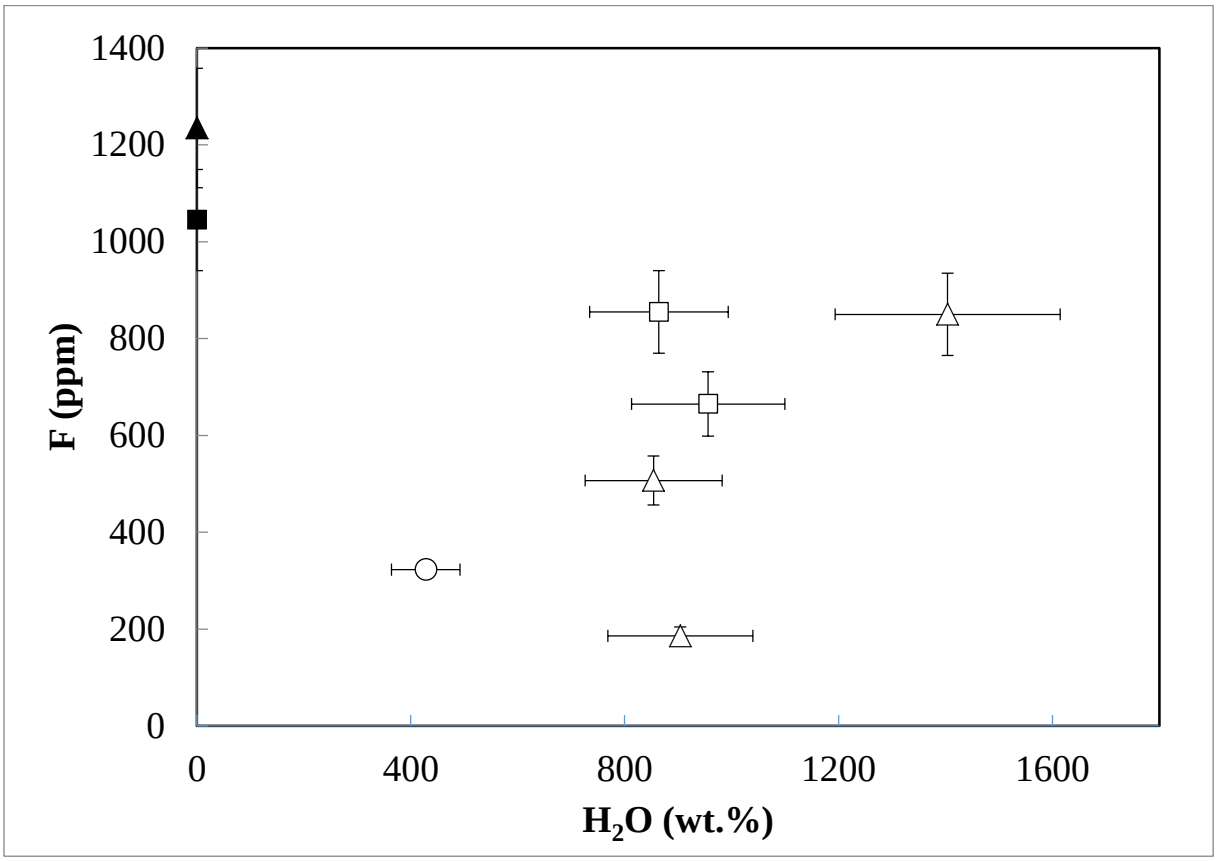

Fig 6

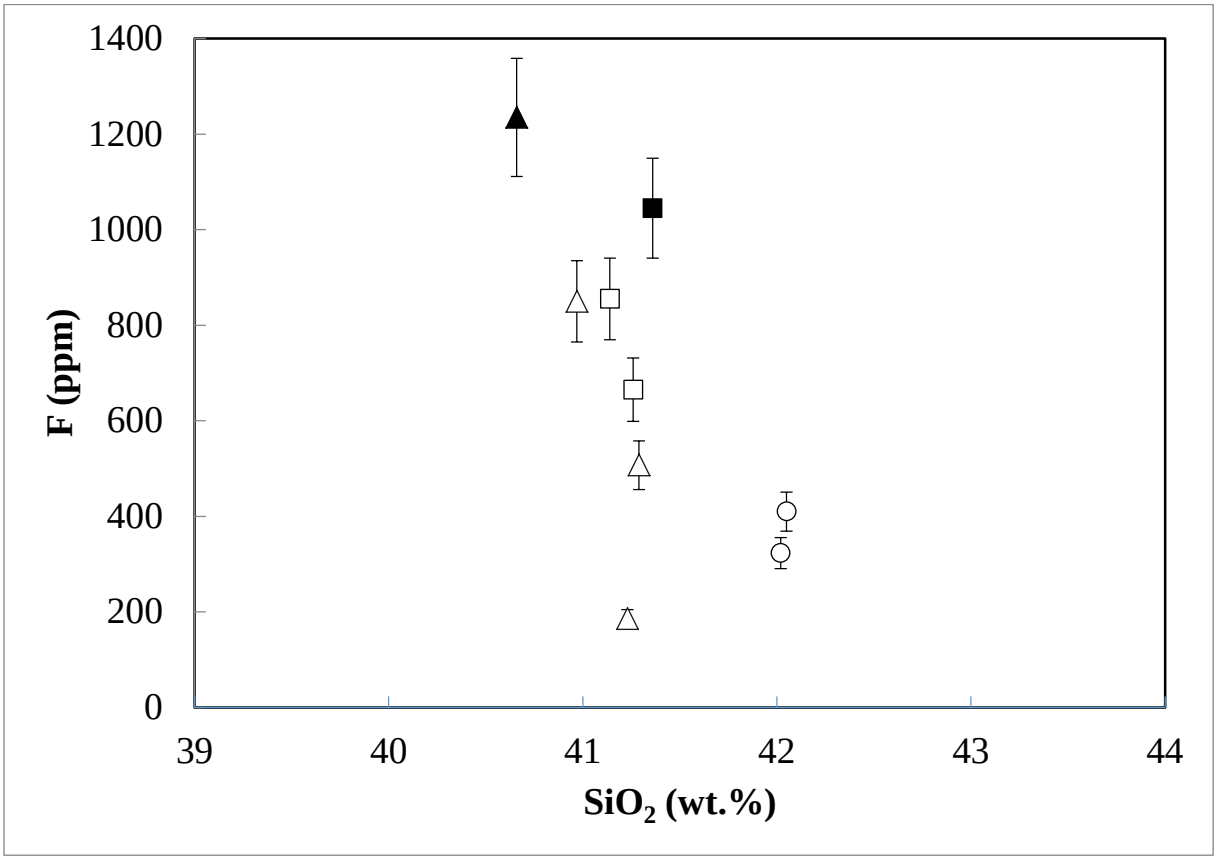

Fig 7

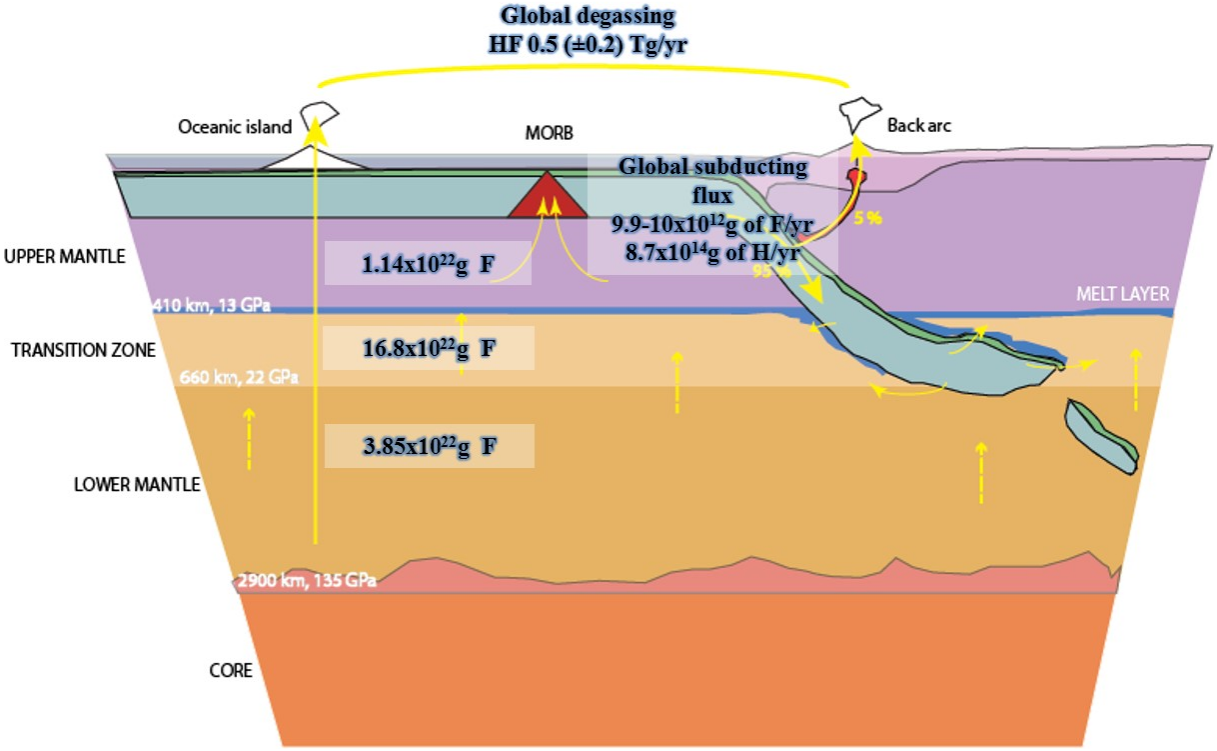
Global degassing
HF 0.5 (±0.2) Tg/yr
Oceanic island
MORB
Back arc
Global subducting flux
9.9-10x10^12g of F/yr
8.7x10^14g of H/yr
5 %
95 %
UPPER MANTLE
1.14x10^22g F
410 km, 13 GPa
MELT LAYER
TRANSITION ZONE
16.8x10^22g F
660 km, 22 GPa
3.85x10^22g F
LOWER MANTLE
2900 km, 135 GPa
CORE

Table 1: Starting materials, experimental conditions and run products

Sample	P (± 1GPa)	T (±50°C)	Time min	Starting Material	Description
San Carlos (SC) powder SCP					Mixture of natural olivine powder +SiO_2
Synthetic Powder SP					Mixture of SiO_2 + MgO + FeO of San Carlos composition
Samples					
83(*)	15	1400	20	Pure SC	Wadsleyite
H3698(*)	22	1400	20	Pure SC	Ringwoodite
87_F(*)	14	1350	420	SCP + 5 wt.% NaF	Wadsleyite (20 µm), enstatite, NaF
H3567(**)	20	1100	240	SCP+ 5 wt.% NaF	Ringwoodite (20 µpm), stishovite, NaF
42_F(*)	14	1400	240	SP + 5 wt.% NaF + 2 wt.% $Mg(OH)_2$	Olivine (70 µm), enstatite, NaF-bearing glass
88_F(*)	14	1400	360	SCP + 5 wt.% NaF + 2 wt.%$Mg(OH)_2$	Olivine (80 µm), enstatite, NaF-bearing glass
40_F(*)	14	1100	240	SP + 5 wt.% NaF + 2 wt.% $Mg(OH)_2$	Wadsleyite (80 µm), enstatite, NaF-bearing glass
H3588(***)	20	1100	240	SCP + 5wt.% NaF + 2 wt.% $Mg(OH)_2$	Ringwoodite 80µm), stishovite, NaF-bearing glass
H3695(*)	22	1250	240	SCP + 5 wt.% NaF + 2 wt.% $Mg(OH)_2$	Ringwoodite (60 µm), stishovite, NaF-bearing glass
H3695(*)	22	1250	240	SCP + 5 wt.% NaF + 2 wt.% $Mg(OH)_2$	Ringwoodite (60 µm), stishovite, NaF-bearing glass
H3696(*)	22	1400	240	SCP + NaF 5 wt.% + 2 wt.% $Mg(OH)_2$	Ringwoodite (60 µm), stishovite, NaF-bearing glass

(*) Au-Pd capsule, (**) Re-capsule, (***) Pt capsule, NaF pure salt, $Mg(OH)_2$, brucite, for all powders : (Mg+Fe)/Si= 1.76. Larger grain sizes in µm are given in brackets

Table 2: Representative analyses of experimental run products and starting natural composition

Sample		Oxides %wt (% rel)												
		SiO_2	FeO	MnO	Al_2O_3	Na_2O	MgO	CaO	TiO_2	Total	Mg #	H_2O ppm (ppm)	F ppm (ppm)	Na ppm (ppm)
References														
San Carlos	Ol	40.34	9.22	0.13	0.01	0.01	49.8	0.08	0.01	99.72	0.90	-	-	-
83	Wd	41.55 (0.09)	9.21 (0.10)	0.12 (0.04)	0.11 (0.02)	0.02 (0.02)	48.48 (0.29)	0.02 (0.03)	0.01 (0.01)	99.63 (0.38)	0.90	-	0	0
H3698	Rw	41.50 (0.31)	9.70 (0.14)	0.12 (0.05)	0.04 (0.04)	0.01 (0.01)	48.79 (0.27)	0.07 (0.02)	0.01 (0.02)	100.39 (0.38)	0.90	-	0	0
Anhydrous														
87_F	Wd	41.24 (0.30)	9.02 (0.19)	0.12 (0.03)	0.09 (0.02)	0.82 (0.09)	48.80 (0.48)	0.02 (0.01)	0.00 (0.00)	100.11 (0.49)	0.91	-	1045 (2)	3145 (2)
H3567	Rw	39.58 (0.11)	11.53 (0.47)	0.13 (0.04)	0.05 (0.04)	0.41 (0.06)	45.67 (0.17)	0.02 (0.01)	0.03 (0.03)	97.42 (0.18)	0.88	-	1235 (5)	2123 (7)
Hydrous														
42_F	Ol	35.41 (3.83)	9.69 (1.87)	0.01 (0.01)	0.05 (0.03)	0.78 (0.33)	54.02 (1.36)	0.01 (0.01)	0.01 (0.01)	99.98 (0.71)	0.93	nd	410 (41)	3230 (323)
88_F	Ol	41.78 (0.27)	3.44 (0.25)	0.10 (0.03)	0.06 (0.02)	0.12 (0.04)	53.86 (0.26)	0.01 (0.01)	0.02 (0.02)	99.39 (0.27)	0.97	428 (65)	323 (32)	713 (71)
40_F	Wd	41.66 (0.34)	8.62 (0.2)	0.04 (0.02)	0.05 (0.01)	0.24 (0.08)	49.91 (0.81)	0.01 (0.01)	0.01 (0.02)	100.54 (0.54)	0.90	956 (132)	665 (67)	2573 (258)
H3588	Rw	40.49 (0.55)	7.67 (0.07)	0.04 (0.04)	0.07 (0.00)	0.09 (0.04)	49.97 (0.42)	0.00 (0.01)	0.03 (0.02)	98.36 (0.30)	0.90	1404 (197)	850 (85)	2503 (250)
H3695	Rw	41.19 (0.29)	10.71 (0.18)	0.10 (0.00)	0.01 (0.01)	0.34 (0.16)	47.64 (0.19)	0.01 (0.00)	0.02 (0.02)	100.02 (0.41)	0.89	904 (127)	186 (19)	1025 (103)
H3696	Rw	40.42 (0.03)	10.61 (0.11)	0.09 (0.02)	0.02 (0.01)	0.39 (0.03)	46.47 (0.14)	0.01 (0.01)	0.00 (0.00)	98.01 (0.04)	0.89	854 (128)	507 (51)	1473 (147)

Oxides wt.% are from EMPA. H_2O ppm from ERDA F ppm and Na ppm from PIGE. Ol= olivine. Wd= wadsleyite. Rw =ringwoodite. Gl= glass. Mg#= Mg/(Mg+Si); uncertainties are given in brackets

Highlights

1. Almost nothing is known about fluorine deep geochemical cycle.
2. Fluorine and water cycles may be closely related in the mantle.
3. Fluorine contents can be significant in wadsleyite and ringwoodite.
4. Large amounts of fluorine may be stored in the transition zone
5. This may provide constraints on the origin of fluorine in the Earth.